High-bandwidth coupling circuit design for PLC applications on SWER networks: From design to production

Engineering Science and Technology, an International Journal 58 (2024) 101840

Contents lists available at ScienceDirect

Engineering Science and Technology, an International Journal

journal homepage: www.elsevier.com/locate/jestch

Full Length Article

High-bandwidth coupling circuit design for PLC applications on SWER networks: From design to production

Kristi Beqirllari *, Cagil Ozansoy, Douglas Gomes, Mike Faulkner

College of Sports, Health, and Engineering, Victoria University, Melbourne, Australia

ARTICLE INFO

Keywords:
Powerline carrier
Coupling circuit
Single-wire earth return
Medium voltage
CENELEC-A band

ABSTRACT

This paper proposes a novel receiver signal-conditioning circuit for Powerline Carrier (PLC) applications in medium-voltage, Single-Wire Earth Return (SWER) networks. The primary aim is to achieve increased bandwidth by lowering the frequency cut-off and leveraging the integrated drain-coil of the coupling capacitor to reduce insertion loss while maintaining signal integrity. The design introduces a flexible trade-off between bandwidth expansion and loss minimization, critical for cost-effectively enhancing communication in complex network environments. Results attested to the feasibility of extending signal reception down to 9 kHz, potentially unlocking previously inaccessible low path-loss areas within the CENELEC-A band. When all stages are engaged, the transmission bandwidth ranges from 27 kHz to 440 kHz for an adjustable insertion loss in the -50 dB to + 0 dB range. Field testing of the design resulted in an SNR greater than 0 dB for 99.99 % of the time, with 98.29 % of measured SNR falling in the 20 dB to 40 dB SNR range. The frequency range, flexibility, cost, and quantitative outcomes assert the effectiveness and reliability of the proposed solution in real SWER network conditions.

1. Introduction

PLC technology can be widely used in power networks for various applications, including ground fault protection [1], smart metering [2], and broadband internet services by utilizing the existing overhead power line infrastructure. Overhead power lines present a significant challenge in efficiently transmitting a signal from a transmitter (TX) to the receiver (RX) while minimizing signal losses and maintaining a high signal-to-no-noise ratio (SNR) at the receiver end. Real-world deployment in SWER power distribution networks faces many challenges, such as the multi-grounded return paths and their bare-conductor configurations, leading to signal dissipation, higher attenuation, impedance mismatches, and increased noise and interference that can degrade the PLC communication signal [3]. The longer transmission distances, high environmental noise, and varying characteristics, such as ground conductivity and network topology, can significantly impact signal propagation, which highlights the need for a coupling design that enables signal reception at frequencies where loss is reduced. An improved design is proposed to allow improved transmission over longer distances and through sections such as underground cable segments. The design flexibility in gain and bandwidth provides an effective solution for adapting to diverse conditions in SWER networks without requiring cost-intensive modifications to coupling capacitors. Given that the CENELEC-A band (9–95 kHz) is often reserved for power utilities [4], Orthogonal Frequency Division Multiplexing (OFDM) can ideally be utilized with reasonable spectral efficiency as a multi-carrier modulation method. The lower portion of the CENELEC-A band can thus be critical for building PLC applications in networks with underground passages that have high capacitance to ground.

Currently, there is a limited number of works in the literature and a shortage of experimentally validated coupling designs for medium voltage (MV) networks. Most existing research focuses on injecting signals into low voltage (LV) networks in smart metering applications. The proposed research addresses this gap by creating and testing a novel RX coupling solution designed for the reception of low-frequency (LF) and wide-bandwidth OFDM signals over SWER lines. This work first investigates a range of PLC coupling techniques, emphasizing their effectiveness in harnessing the lower frequencies (9 kHz to 60 kHz) of the CENELEC-A band. Then, it proposes a design methodology for coupling a PLC receiver to the MV line as its main contribution. In testing the application, TXs are connected to the LV side (240 V) of the SWER transformers, and the RX is coupled to the MV (12.7 kV) using a drain-coil integrated coupling capacitor (CC). The central feature that sets this methodology apart from other works is its ability to enable signal reception at frequencies potentially as low as 9 kHz. In this paper, the authors present and discuss the design, build, and field test of a coupler with a target frequency cut-off (fc) of 17.5 kHz. While the

* Corresponding author.
E-mail address: kristi.beqirllari@vu.edu.au (K. Beqirllari).

https://doi.org/10.1016/j.jestch.2024.101840
Received 26 April 2024; Received in revised form 23 July 2024; Accepted 11 September 2024
Available online 2 October 2024

design is based on a CC with a 5.11 nF capacitance and a drain coil of 0.223 mH, the method can be adapted to other capacitor and drain coil values to maximize performance. The methodology focuses on capacitive coupling methods, giving their predominant use in this field, although the authors intend to investigate, compare and generalize the coupling design for inductive methods in future works. The key contributions of this work, distinguishing it from prior publications, are:

- A coupling circuit has been designed that extends signal reception down to 9 kHz, unlocking the lower portion of the CENELEC-A band, making the low path-loss section of the band available for transmission and enabling potential PLC applications over high-loss networks at higher frequencies, such as those containing underground sections.
- A modular signal conditioning circuit with four stages: wideband coupler, attenuation, filtering, and amplification. The resulting bandwidth ranges from 27 kHz to 440 kHz, with an adjustable insertion loss in the −50 dB to +0 dB range.
- Field testing of the design on real networks, resulting in an SNR above 0 dB for 99.99% of the time, with 98.29% of measured SNR falling in the 20 dB to 40 dB range.
- A novel design that compensates for the impact of the drain coil of MV CC on the available bandwidth, incorporating a series RC impedance in parallel with the drain coil to create a resonant circuit dropping the lower cut-off frequency.

2. Literature review

Several studies have examined the current state of PLC technology that identify its limitations and propose potential solutions [5–7]. These efforts highlight the ongoing work to improve the efficiency and reliability of PLC systems in practical applications. Publications by [8,9] have explored the essential role of impedance matching and signal injection in improving PLC performance.

Impedance matching aligns the impedance of the signal source with the power line, maximizing power transfer and minimizing reflections. Maintaining reliable communication is significantly challenged by the electrical networks' harsh environment, marked by a frequency- and load-dependent access impedance behavior and dynamic background noise due to switching events and equipment malfunctions [10,11]. The ease of measurement and integration in LV power lines, combined with restricted access to MV SWER lines, has led to numerous studies on LV PLC systems [12–17], primarily focusing on home automation and smart metering. The propagation distance of the signal is determined by the access impedance of the LV electrical grid, making the design of PLC device interfaces to the grid a critical aspect of system performance. The injected voltage of transmitted signals is affected by the impedance mismatch between the transmission device and the grid access impedance [8,12,18]. Although LV power lines present challenges such as numerous branches, close proximity to noise sources, and complex load profiles, their short distances and straightforward coupling methods make them advantageous for multimedia applications and home networking [5,19–21]. On the other hand, the deployment of PLCs at the MV level is less prevalent due to various technical challenges associated with grid characteristics. MV networks and secondary substations exhibit diverse configurations, necessitating careful consideration of multiple factors for robust signal interfacing. These factors include the type of physical coupling, voltage and impedance levels, frequency bandwidth, propagation modes, and the number of connections [3,22,23]. Various methods for PLC signal coupling include capacitive, inductive, resistive, antenna or a combination of two or more of these methods to optimize signal coupling for specific applications and conditions [5,6].

Inductive coupling offers several advantages for power-line communication systems. It eliminates the need for direct physical connections to live power terminals, thus reducing the risk of electric shock. Inductive couplers perform well at low power-line impedance levels, maintaining high signal integrity with minimal loss and distortion [14,16,17]. Rensburg et al. [24]. have shown a step-by-step design of an inductive coupler for LV networks, operating at narrowband frequencies from 100 kHz to 1 MHz, covering the European CENELEC-B, C, and D bands. Measurements with different cable lengths indicated that attenuation for a 40 m length cable varies between 20 to 30 dB [24]. Sohn et al. [25,26] have demonstrated that inductive coupling can be successfully employed in in-vehicle power line communication. The inductive coupler operates efficiently within a broadband frequency range of up to 40 MHz. These results are similar to those reported by Kim et al. [27], who examined the signal transmission properties of inductive couplers using high permeability magnetic materials and found that these materials maintained a flat insertion loss of −5 dB in the 5–40 MHz frequency range, confirming the suitability of inductive coupling for high-frequency broadband PLC applications in EVs.

While inductive coupling offers significant advantages for high-frequency broadband PLC, capacitive coupling presents another viable method, particularly in LV and MV networks [7]. Capacitive coupling devices for PLC systems offer significant advantages, particularly for LV and MV networks. These cost-effective interfaces are simple to integrate into existing infrastructures and include features such as a 50 Hz filter and grounding resistance to minimize noise, enhancing reliability for AMI and smart grid applications [28–32]. Notably, these devices support various transceiver technologies, emphasizing their versatility within LV networks [22,33,34]. Both Razazian et al. [35] and Costa et al. [36] documented substantial frequency-dependent attenuation within the 35 kHz to 90 kHz range for narrowband signals in MV networks, posing challenges to achieving reliable communication in the lower CENELEC-A band frequencies. Research on a hybrid coupling method, which integrates both capacitive and inductive coupling techniques, was documented in studies [13,37,38], focusing on practical testing within small-scale networks. Artale et al. [39–41] introduced two new concepts for coupling PLC signals to MV lines using the capacitive divider functionality of Voltage Detecting Systems (VDS) and commercial separable connectors (SC) in MV cable heads. Despite innovative approaches for signal injection and reception, the authors faced significant attenuation in the lower frequencies of the CENELEC-A band.

2.1. Summary of findings

The evaluation of some studies by Cataliotti et al. [42] and Oh et al. [43] was limited to small overhead networks, which constrains the analysis of the proposed circuits' efficacy in larger networks. The literature review indicates that increased attenuation at the lower frequencies of the CENELEC-A band has prevented researchers from utilizing this portion for communication purposes. Due to the internal drain coil effects in coupling capacitors, most research by Lee et al. [44], Artale et al. [39–41] and Benato et al. [45] focuses on higher frequencies within the CENELEC-B and upper CENELEC-A bands, starting around 60 kHz. Coutinho et al. [5] noted that 94% of PLC research concentrates on LV networks due to their accessibility, simpler coupling methods, and shorter distances. Additionally, they found that 90% of these studies focus on broadband PLC (BB-PLC), with only 10% addressing narrowband PLC (NB-PLC). This highlights the necessity of expanding research efforts to cover medium-voltage applications and to improve the understanding and development of NB-PLC technologies. To advance PLC technologies, future research should address the challenges and limitations observed in current studies, particularly focusing on medium-voltage networks and the utilization of lower frequency bands.

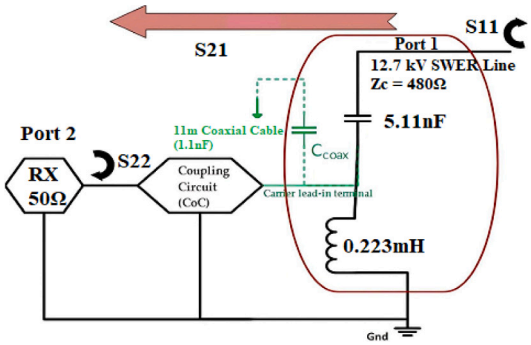

Fig. 1. Full system diagram showing the coupling of a PLC receiver to the MV line through a CoC and a drain-coil integrated CC. The access impedance (encircled in red) consists of the capacitance of the 11 m coaxial cable, a 5.1-nF rated CC with a drain coil of 0.223 mH, and the 480 Ω Z_c of the line. The CoC sits in between the RX and access impedance and seeks to yield a flat frequency response for the received signal.

3. Design methodology

The first critical parameter that must be analyzed when designing coupling interfaces for MV lines is the characteristic impedance of the line, Z_c. Lee et al. [46] verified that Z_c of an MV power distribution line is 400 Ω to 600 Ω in the 1 MHz to 40 MHz frequency range. Equations relating Z_c to line attributes such as inductance and capacitance per meter, etc., can be traced to the time-dependent telegrapher's model and are described in [47,48]. The reader can refer to the works in [30, 49] for alternative proposals for modeling SWER distribution lines. Here, the characteristic impedance was based on the line model theory and the design process on the IEEE standard [50], which covers the bandwidth from 0 to 500 kHz. Z_c is frequency-dependent at very low frequencies but settles around ≈480 Ω as frequency increases, which is the value adopted here.

A CC allows PLC signals to enter the carrier equipment by providing a low-impedance path to high-frequency (HF) signals while attenuating the fundamental (50 Hz). There are two main commercially available CC structures. The first uses the CC in a capacitor divider network as a voltage transformer, which is often used for measurement purposes. The second uses the CC with an integrated drain coil. In [51], the carrier drain coil is specified as a requirement in all CCs with carrier accessories since it provides a low impedance to ground for the power frequency (50 or 60 Hz) currents and a high impedance for PLC signals. A larger drain coil inductance is needed for the low end of the PLC-frequency range (below 70 kHz), while smaller inductance values are acceptable for the higher frequency ranges. Fig. 1 shows the 50-Ω RX interfaced to a 12.7-kV MV line having a Z_c of 480 Ω. The overall access impedance, looking into port 2, consists of the capacitance of the 11-m coaxial connection cable (capacitance to ground shown in Fig. 1), an off-the-shelf 5.1-nF rated CC with integrated 0.223-mH drain coil, and the 480 Ω Z_c of the line.

The process of designing a wideband CoC with a flat frequency response commences by examining the transmission coefficient (S_{21}). The second step involves modeling the CC on Microwave Office to explore the CoC design space in a semi-iterative, semi-analytic approach. In the third phase, over-voltage and over-current (OV/OC) protection elements are incorporated to safeguard against potential harm. After the design and simulation phases, the PCB is manufactured adhering to high-frequency (HF) signal conditioning guidelines. After building the PCB, it undergoes rigorous testing in a controlled lab environment, comprising all components slated for deployment in the field. The hardware later undergoes field tests to ensure that the designed circuit performs appropriately under operational scenarios.

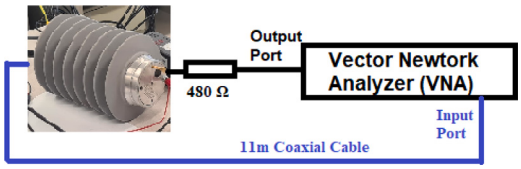

Fig. 2. S_{21} measurement set-up of the CC, including a 480-Ω resistor simulating the Z_c of the MV line, the 5.1-nF CC, and the 11-m coaxial cable.

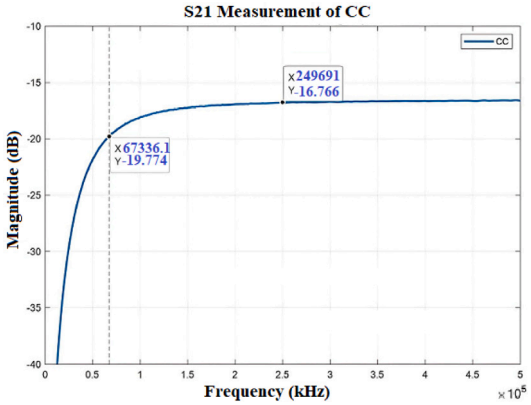

Fig. 3. Measurement of the CC's S_{21} transmission coefficient (insertion gain) with a vector network analyzer, showing a cut-off (f_c) frequency of 67 kHz and a passband insertion loss of 16.7 dB.

3.1. Limitations of capacitive coupling in PLC applications

The first measurement employed a Vector Network Analyzer (VNA) to conduct a frequency sweep of the CC's insertion gain (S_{21}). The schematic diagram of the test set-up detailing this measurement is depicted in Fig. 2. To emulate Z_c of the power line as per the IEEE P1901-2 standard [50], a 480-Ω resistor was inserted in series with the MV side of the CC. Fig. 3 shows the S_{21} characteristic of the utilized 5.1-nF CC. The high-pass cut-off frequency (f_c) is ≈ 67 kHz, with attenuation increasing at frequencies below, reaching ≈ −140 dB at 50 Hz, which is enough to suppress the line voltage into the mV region at the CC output.

For the analysis of the characteristics of the CC, a simulation model (see Fig. 4) was built in Microwave Office AWR to model its frequency response. As in Fig. 5, the voltage gain characteristics of the CC model (blue trace), as constructed within the Microwave Office AWR, closely mirrors the frequency response observed in empirical measurements showcased in Fig. 3. Note that Fig. 3 shows the CC transmission coefficient (insertion gain), while Fig. 5 is the Voltage Gain from Input Voltage Source (VSG) measurement. This congruence in the frequency response is noteworthy, as it reveals an f_c of 67 kHz. This alignment between the model's behavior and measurements validates the model's accuracy and underscores its suitability for a variety of simulation-based testing scenarios.

Particular emphasis is paid to the simulation of the CC model with different drain-coil inductance values. In line with the recommendation in [51], f_c could be lowered to around 54.6 kHz by increasing the drain-coil inductance to 2 mH. Any further improvements would require an increase in the CC capacitance; both options are costly. The key intention here is to establish how such a bandwidth improvement could be cost-effectively achieved through improved coupler design. The 5.11-nF CC is designed for broadband PLC applications that use frequencies above 2 MHz. This was the major motivation for the investigation of a CoC design to extend the frequency range down to the lower CENELEC and FCC frequencies.

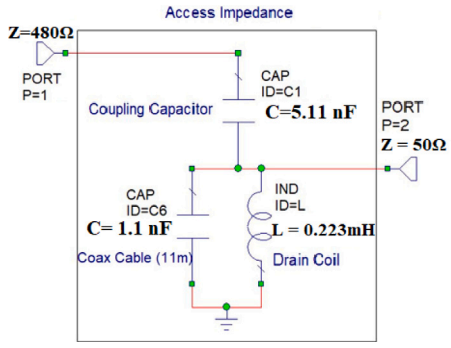

Fig. 4. CC modeling demonstrating the internal circuit composition of a drain-coil integrated CC.

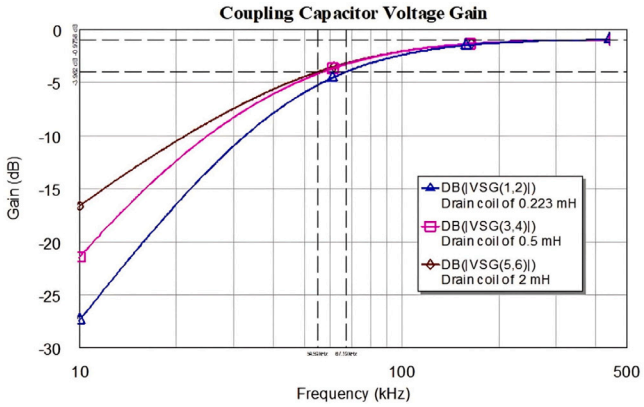

Fig. 5. Voltage gain from Input Voltage Source (VSG) measurement of the CC simulated for different drain-coil inductance values. The figure shows that f_c could be lowered by increasing the drain-coil inductance to 2 mH.

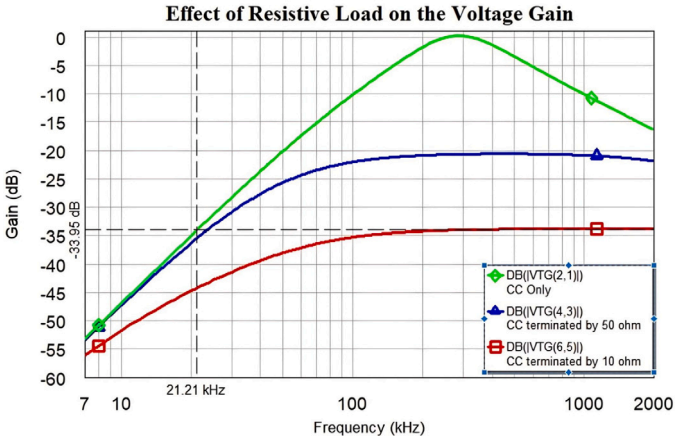

Fig. 6. Effect of load resistance on CC voltage gain vs. frequency. The source impedance is 480 Ω. From top: no-load (green) with f_c=179 kHz; 50 Ω load (blue) with f_c=67 kHz; and 10 Ω load (red) with f_c=61.5 kHz,.

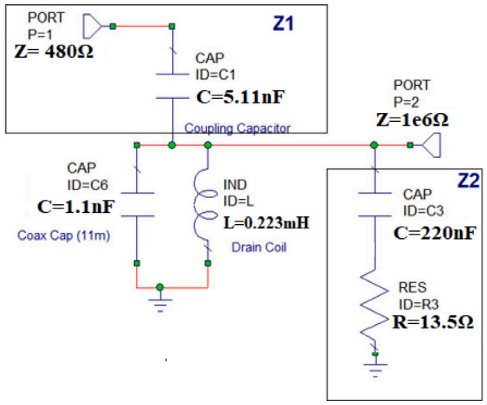

Fig. 7. The addition of a series RC impedance (Z_2) makes the attenuation set by the voltage divider $Z_2/(Z_1+Z_2)$ constant for all frequencies, flattening the frequency response.

4. Wideband coupler design (Equalizing Circuit)

The design philosophy trades off increased bandwidth for reduced signal gain. The gain reduction is not a problem for signal reception at these frequencies since signal levels can easily be recovered with subsequent amplification (if required). The noise penalty for doing this is minimal since the PLC channel noise is high and will always dominate any small contribution from the receive amplifier's noise figure. Fig. 6 shows the effect of different loading conditions on the CC driven from a 480-Ω impedance MV source. The 11-m coaxial cable (C6) is included as part of the CC as per Fig. 4.

The green (top) plot shows the signal gain when the output (Port 2, Fig. 4) is high impedance (open circuit). The 0 dB resonance peak between the drain coil and C6 occurs at 280 kHz for which the 3 dB lower cut-off is 179 kHz. C6 is also responsible for the high-frequency roll-off of the curves but has little effect below 500 kHz after loading is applied. When the output load on Port 2 is reduced to 50 Ω, the cut-off frequency, f_c, drops to 67 kHz for a passband loss of 20 dB (blue curve). The direct connection to high-frequency 50-Ω cables is possible and makes this CC suitable for Broadband PLC transmissions into MHz frequencies. A further reduction in Port 2 loading to 10 Ω gives a small f_c improvement to 61.5 kHz but at the expense of a further 14 dB of attenuation (red curve). These curves have reasonably flat pass-bands, but their initial drop-off is gradual and asymptotically bounded by the original high impedance (green) response with a 40 dB/decade slope. The goal is to extend the lower bandwidth for a given attenuation to at least the high impedance (green) curve, as indicated by the −34 dB dashed lines for the 10-Ω load case. As the green line represents the high impedance (1×10^6 Ω) loading of the CC, which is an ideal scenario, further extension beyond the high impedance curve is not trivial. Considering that the Port 2 loading will not be so high when the RX circuit is connected (loaded), any further reduction in the lower cut-off frequency is unfeasible. Reducing load impedance improves the cut-off frequency but increases attenuation, highlighting the challenge of balancing bandwidth extension and signal attenuation.

The design process begins by adding a series RC impedance (C3 and R3 in Fig. 7) in parallel with the drain coil to create a resonant circuit tuned to the frequency where the selected attenuation crosses the green high-impedance CC response line (≈21.2 kHz in Fig. 6). Fig. 8 (blue curve) shows the impact of C3 and R3 on the Voltage Gain from Input Terminal (VTG) from Port 1 to Port 2. The drain coil, L, and C3 determine the resonant frequency, $f_{res}=\frac{1}{2\pi\sqrt{LC}}$, while R3 controls the gain at high frequencies $R3/(R3+Z_c)$ to approximately −31 dB. The practice of adding the low-voltage $C3+R3$ combination in parallel with the drain coil is at the heart of maximizing the CoC usable bandwidth for drain-coil integrated CCs. This cost-effective principle assists in lowering f_c without necessitating an increase in the capacitance of the CC or the inductance of the drain coil. The series impedance of C3 and R3 (Z2) helps to make the attenuation set by the voltage divider $Z2/(Z1+Z2)$ constant for all frequencies resulting in a flat frequency response. Note Z1 is the line impedance (Z_c = 480 Ω) in series with the CC (C1). The ratios Z_c/R3 and C3/C1 are therefore set relatively close. As shown by the blue trace in Fig. 8, there is still a challenge to address, which relates to the resonance observed in the frequency

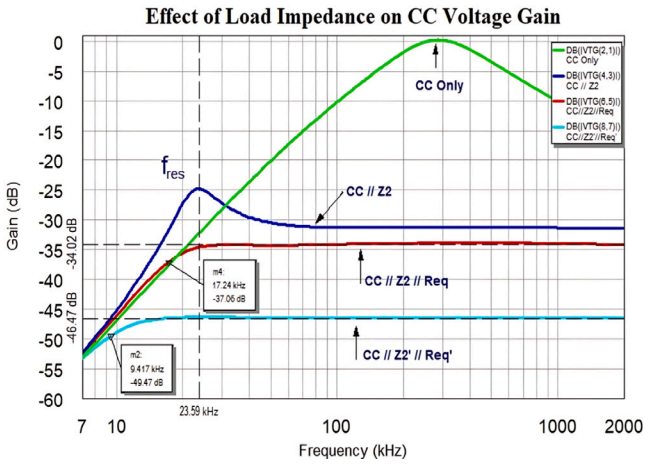

Fig. 8. Effect of load impedance on CC voltage gain vs. frequency, with source impedance equal to 480 Ω. From top: No-load (green); load = Z_2 Ω (blue); load = $Z2 \parallel R_{eq}$ Ω resulting in f_c = 17.5 kHz (red); and load = $Z_2' \parallel R_{eq}'$ Ω resulting in f_c = 9 kHz (turquoise). Where ($Z_2 = R_3 + jX_{C3}$) with component values from Table 1.

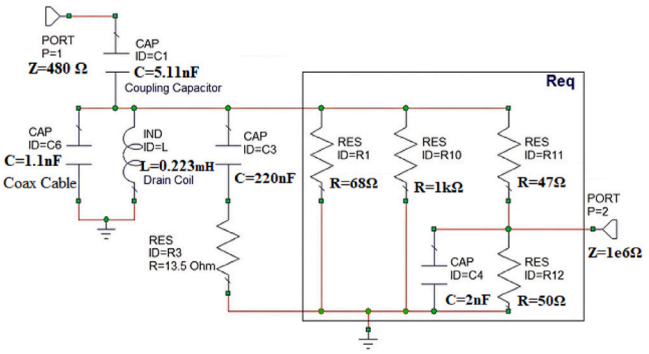

Fig. 9. Design using R_{eq} to reduce resonance for a sharp cut-off and reduced f_c.

Table 1
Coupling circuit component values.

f_c (kHz)	Gain @ 200 kHz	f_{res} (kHz)	C3 (nF)	R3 (Ω)	R_{eq} (Ω)	R5 (Ω)
17.5	−34 dB	21.2	219	13.5	39	68
9.4	−46.5 dB	11	880	2.8	12.8	15

response. This effect can be damped by adding a resistor to ground (R_{eq}) implemented as a parallel combination of R1 ∥ R10 ∥ (R11+R12) as shown in Fig. 9, followed by small tweaking of R3 and C3 for a flat response. The result is the elimination of the resonance that was unavoidable using Z2 only (Fig. 8 red) but at the expense of a small gain reduction to −34 dB. Nevertheless, a comparison between the red curve of Fig. 6 (10-Ω resistor loading), which has the same gain (−34 dB), shows a cut-off frequency reducing from 61.5 kHz to 17.5 kHz, and a bandwidth increase of 44 kHz, emphasizing the effectiveness of the resonance approach.

Finally, to demonstrate the flexibility of this approach, the bottom curve (Fig. 8 turquoise) shows the design of a coupling network that covers the entire CENELEC-A band down to ≈9 kHz. Table 1 gives component details for both designs. As the lowest sections of the CENELEC-A band usually present high noise levels and are often not used, hardware implementation was based on the f_c = 17.5 kHz values.

The CoC schematic is shown in Fig. 10. C3 was divided into two different capacitors for better selection from standard capacitor values. While the resonant circuit counteracts the drain coil, lowering f_c, the compensation circuit ensures consistent gain.

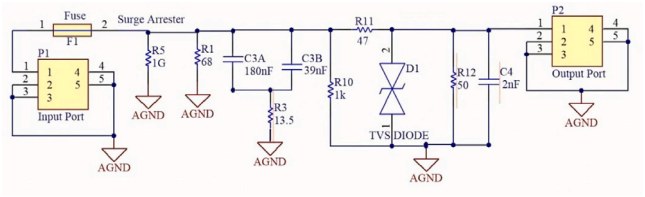

Fig. 10. Coupler Circuit's Altium schematic diagram.

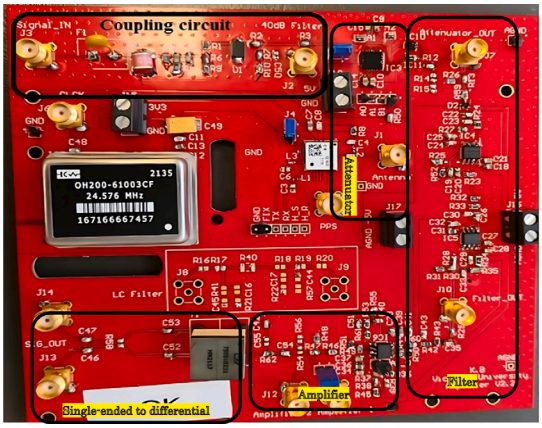

Fig. 11. Detailed PCB circuit implementation of the overall signal conditioning circuit.

The circuit includes over-current and over-voltage protection features: a reversible fuse (F1), a gas discharge surge arrestor (R5) for spike protection and a bidirectional transient voltage suppression (TVS) diode that limits excessive voltage by diverting it to ground. SMA connectors terminate the network (P1, P2). The primary reason for the output circuit components R11, R12 and C4, therefore, is circuit protection. The 50-Ω termination (R12) is only necessary if the subsequent stage is high impedance, which here is removed for 50 Ω input stages. R11 (47 Ω) provides an impedance for the TVS coupling, and C11 provides suppression of very high frequencies outside the control range of the active filter stages. There is a ≈6 dB additional loss through the output circuit.

As already indicated, altering f_c also affects the gain, as there is a trade-off between gain and bandwidth. The RX conditioning board circuitry shown in Fig. 11, integrates a fully remote-controllable amplifier-attenuator stage, as solution to address this loss. Additionally, the circuitry is equipped with a configurable frequency band-pass filter and a selectable output that can be either single-ended or differential, accommodating various ADC configurations.

5. Coupler laboratory measurements

The next step involves measuring the output response of the CoC cascaded with the CC and its 11-meter coaxial cable. This was undertaken using a VNA as previously presented in Fig. 2, with the CoC included. Fig. 12 compares the signal's behavior when the CC operates in isolation to when it is integrated into the system along with the wideband CoC. Trace 2 (orange) displays the graphical representation of the frequency response of the cascaded CC and CoC combination. The design demonstrates the anticipated bandwidth improvement compared to Trace 1 (blue) from the S_{21} response of the CC without the CoC. With trace 2, we observe the mid-band attenuation level of −36 dB and cut-off frequency (f_c) of ≈19 kHz, close to the predicted 17.5 kHz. The small differences are caused by the component tolerances and the inclusion of the protection components. The result is that, by incorporating the CoC, an additional 48.5 kHz of bandwidth becomes accessible, enabling transmission waveforms based on power line characteristics (attenuation, noise, etc.).

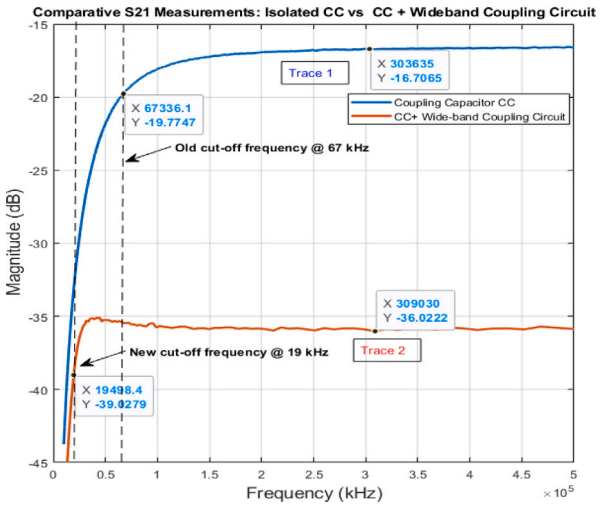

Fig. 12. S_{21} measurements of the CC cascaded with the CoC. Trace 1 (blue) CC on its own with f_c= 67 kHz. Trace 2 (red) CC and CoC reducing f_c to ≈19 kHz with a gain of −36 dB.

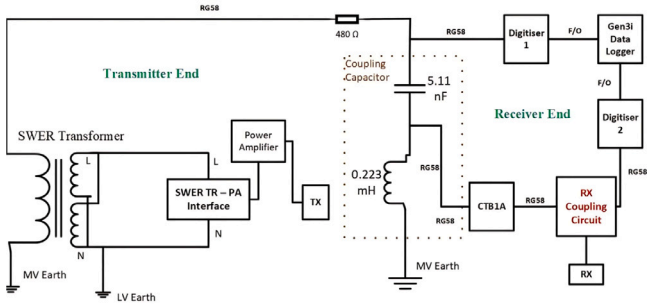

Fig. 13. A diagram of the laboratory test rig demonstrating (i) the coupling of a TX to the LV winding of a SWER transformer through a mains interface and a power amplifier, (ii) MV to RX coupling through the CC with integrated-drain coil and RX CoC. Digitizers and Data Logger record the voltage at the input of the CC and at various ports on the CoC. CTB1 A is a spark gap protection box.

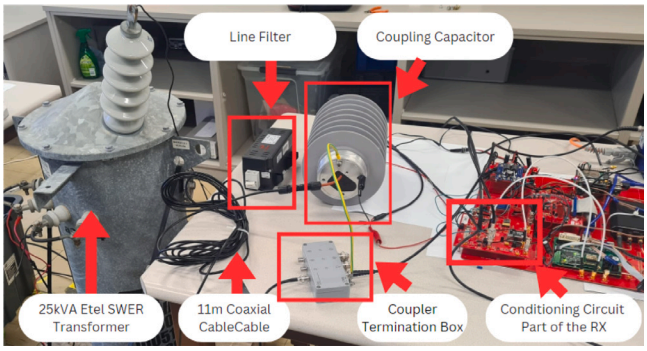

Fig. 14. Complete Laboratory Setup of the SWER MV System. This setup includes an MV transformer, a power line, a coupling capacitor, the CTB1 A Coupler Termination Box, and the RX conditioning board, illustrating the full configuration used for signal testing and analysis.

6. Laboratory test Rig for Point-to-Point analysis

The design of an electronic circuit for receiving signals from outdoor MV transmission lines involves high voltages, which inherently pose safety risks requiring the coordination of numerous specialized individuals and resources. The initial testing was therefore performed in a laboratory without the MV, with the emulation of close conditions

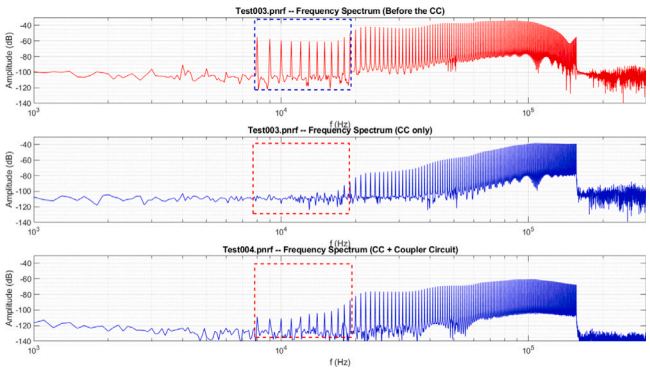

Fig. 15. Results from the laboratory test rig. Top: input signal from the line to the CC. Center: signal received at RX without the coupler circuit. Bottom: signal received at the RX with the coupler circuit. The out-of-band sub-carriers are shown boxed.

to the anticipated environment (Fig. 13). The TX side includes the transmitter, amplifier, and 240 V interface through a 25 kVA (12.7 kV to 240 V) SWER transformer. The RX side includes the CC, wideband CoC, and RX as shown in Fig. 14. The transmission line was modeled with its characteristic impedance, Z_c. The system incorporates two digitizers feeding a transient recorder. This dual-digitizer arrangement enables the simultaneous capture of two critical signal recordings: the voltage signal at the MV input of the CC and at various points within the CoC. This comparative analysis has enabled authors to discern the exact impact of the CoC on the signal. The final measurements of the CoC prior to its field installation are illustrated in Fig. 15. In these measurements, an OFDM multicarrier signal spanning from 8 kHz to 156 kHz was generated by the TX, amplified, and injected through a SWER transformer. The transmitted signal is captured at the receiver side through the CC.

The top plot in Fig. 15 shows the frequency response measured on the HV terminal of the CC. It is evident that the generated signal is affected by impedance variations going through the amplifier, the transformer LV to MV coupling, and the loading effect of the CC. There is a 30 dB range between the strongest and weakest in-band (19 kHz to 150 kHz) sub-carriers, the latter due to the dip at ≈140 kHz caused by the CC-drain coil series resonance. In Fig. 15, the center plot shows the signal received at the RX when the output of the CC is directly connected to the RX without the coupling circuitry. As expected, the internal drain-coil inductor further attenuates the lower-frequency sub-carriers. This difference between the strongest and weakest in-band sub-carriers is now 46 dB, with the lowest 8 sub-carriers being below the noise floor. The bottom plot shows the case where the proposed CoC is cascaded to the CC, and the output to the RX is taken from the output port of the wideband CoC. The difference between the strongest and weakest in-band sub-carriers is now improved to 20 dB. In addition, compared to the center plot, frequencies below 19 kHz are now definitely visible and above the noise floor even though they are in the stop band ($< f_c$). Note the depression in the noise floor, particularly below ≈50 kHz, contributes to the improved signal-to-noise ratio, which is an improvement in signal reception taken as a key benefit of this proposed design. As the CC+CoC combination has a flat response (+/−0.5 dB), any residual in-band frequency response (Fig. 15 bottom) is generated by the transmitter site. The LV-to-MV transformer coupling is the prime cause, which, as indicated, is very frequency-selective.

It is noteworthy that there are two main factors contributing to the noise. One is the noise and interference components picked up from the laboratory. The other is given by the FFT processing leakage when calculating the spectrum plots. As the digitizer was not synchronized to the transmitter, the transmitted frequencies did not fall exactly into the frequency bin structure of the digitizer's FFT, leading to a

leakage floor roughly proportional to the signal strength. Here, the leakage component is approximately 40 dB below the signal level and dominates the noise for all but the smallest of input signals.

7. Research impact

The key driver for this research was the need to design a signal conditioning circuit including a CoC to receive PLC transmissions at the lower end of CENELEC-A band. This sought to overcome challenges in maintaining reliable transmission in overhead networks incorporating underground sections. A pertinent characteristic of one of the trial networks was a 370-meter underground link within an overhead 5.4-km path, as highlighted in the project public report [52]. Underground cables have high capacitance and low characteristic impedance, which adversely affects the reflection coefficient (lowers the transmission coefficient) at the interface of the overhead, $Z_c \approx 480\ \Omega$, and the underground section, $Z_o \approx 35\ \Omega$. PLC signals thus experience additional reflection losses when traversing such an interface. To compensate for this loss, the OFDM modulation needs to be down-banded to exploit the reduced line losses available at lower frequencies. Fig. 16 shows the received 5 sub-carrier signals occupying the 30 kHz to 40 kHz band. Signals transmitted at frequencies above 50 kHz were undetectable despite using the same power per sub-carrier from the transmitter site. Note that the 30 kHz lower limit was set by the bandpass filter of Stage 3, not at Stage 1 of the CoC. The redesign of the coupling system discussed herein would enable reception at even lower frequencies despite utilizing a CC and drain coil combination that is more suited to high-frequency Broadband PLC signals. To validate its effectiveness, the results of testing the design over a week period are discussed. Fig. 17 shows the SNR measurements of the received signal after its demodulation and cross-correlation. During this period, the demodulation was evaluated approximately 30,414,150 times. The analysis resulted in some central findings: (i) minimum SNR was −2.98 dB, and the maximum SNR was 45.46 dB, (ii) SNR was less than 0 dB for only 0.000148% of the time, and (iii) SNR was in the 20 dB to 40 dB range for 98.29% of the time, demonstrating consistent quality signal reception. These figures assert the coupling circuit's effectiveness in conditioning the signal received from the power line, filtering out unwanted noise and interference, and improving the quality of the received signal. By proper impedance matching (in Stage 1) between the 480-Ω power line and the 50-Ω RX, it successfully maximized signal transfer while minimizing reflections.

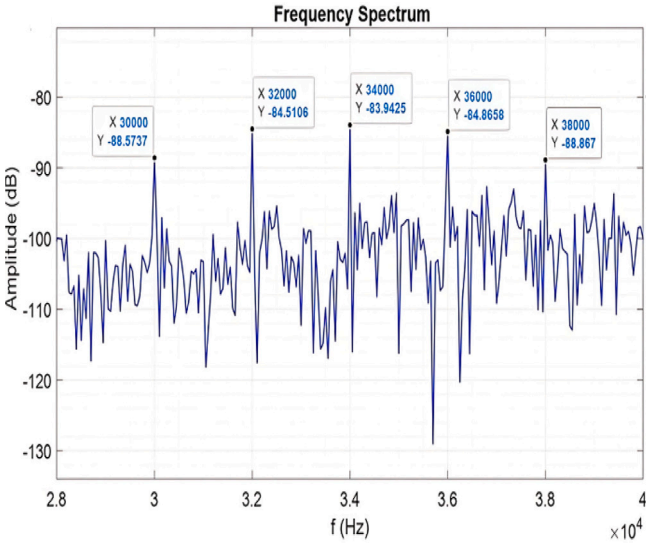

Fig. 16. The received 5 sub-carrier OFDM sequence from a 5.4-km overhead system having a 370-m underground section.

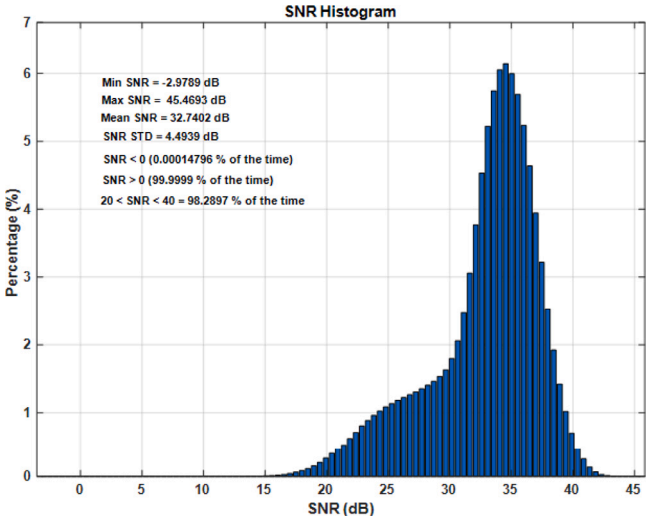

Fig. 17. SNR histogram of the demodulated signal reception over a week period showing an SNR greater than 0 dB 99.9999% of the time.

8. Discussion and comparative analysis

As elaborated in Table 2, it is evident that few designs have achieved frequencies below 35 kHz, largely due to the inherent characteristics of the internal circuitry within the CCs. Monitoring applications often use a small CC ($\approx$ 1 nF) in a capacitive voltage divider structure. Operation at low PLC carrier frequencies has a contrast challenge given by the high impedance CC and the low impedance of the capacitor of the divider network connected to ground. Communications in the CENELEC band, therefore, involve introducing a parallel inductor to resonate out the low impedance of the grounded capacitor, which limits the transmission bandwidth. Further, the small CC makes low insertion loss difficult, as shown by Refs. [29,39,40,42] in Table 2. An alternate CC structure uses an internal drain coil to suppress the line voltage, as per the IEEE international standard [50]. This is an adequate solution for broadband PLC as indicated by [43] of Table 2. The coupling capacitor used in this work (5.11 nF + 0.223 mH) was indeed purchased from a broadband PLC manufacturer. However, wideband operation at the lower narrowband PLC frequencies remains difficult unless the CC value and drain coil values are increased, which is an expensive alternative. Previous works discussed here can be used as examples. Kikkert [30–32] used larger coupling capacitors (12 nF) and a much higher impedance drain coil (1 mH) to get frequencies down to ≈35 kHz, enough bandwidth for G3-PLC; Costa et al. [36] presented good results down to 42 kHz, also from a specialized design.

Recent studies in coupling technologies have identified several design challenges. Costa et al. [9] and Artale et al. [41] demonstrate challenges in maintaining flat frequency responses across their operational bandwidth. The design described in [9] necessitates additional equalization to compensate for variable attenuation, whereas the system developed in [41] achieves a flat response within a restricted FCC frequency band. However, the absence of field testing restricts its validation under real-world conditions. Furthermore, inductive coupling in [23] and capacitive coupling in [34] both exhibit significant signal attenuation issues that exceed 30 dB, compromising signal integrity over longer distances. In [34], necessary amplification is required to compensate for the signal attenuation at low frequencies. The design from [22] is restricted to a 12 kHz bandwidth, limiting its application to specific channel measurements at LV and MV. The limited bandwidth and variable attenuation reduce system performance and reliability.

Two off-the-shelf tuning products are used for a brief comparison to highlight the proposed design flexibility. The MCD80 is marketed

Table 2
Comparison of research accomplishments with other MV coupling works.

Reference	Coupling type	Frequency range	Performance metrics	Applicability
Cataliotti [29,42]	Ohmic-capacitive divider. Undisclosed values	3 kHz	Insertion loss is 6 dB. Very narrow bandwidth, at 86 kHz.	For Cable Networks (Zo=35-Ω to 45-Ω).
Oh [43]	Capacitor with drain coil	1 MHz to 35 MHz	Insertion loss is 18 dB.	Not within the CENELEC Frequency range. Uses Ruthroff wideband impedance transformer
Kikkert [30–32]	Capacitor with drain coil, Bespoke highpass structure	35.9 kHz to 500 kHz	Insertion loss is 1.2 dB	Requires large MV coupling cap (12 nF) and large drain (1 mH) coil. Expensive.
Artale [39,40]	Capacitive divider from a voltage detection system.	102 kHz to 117 kHz	Insertion loss is undisclosed. Low bandwidth	For Cable Network. Variable inductance resonates out the grounded capacitor.
Costa [36]	Capacitor with Drain Coil. Additional integrated features	42 kHz to 89 kHz	Insertion Loss Undisclosed	Specialized Circuit incorporating line output for powering communications equipment.
Costa [9]	Capacitive Coupling.	300 kHz to 1 MHz	Not fully flat response across the frequency range, leading to varying attenuation. Additional equalization might be needed	Suitable for high-frequency applications in IoT and low-voltage power grids.
Artale [41]	Capacitive divider (MV Cable Head)	FCC frequency band (154.6875 to 487.500 kHz)	Flat response within 80 kHz bandwidth, SNR of 25 dB	Medium Voltage (Laboratory tested only, no field tests conducted).
Nogueira [23]	Inductive Coupling.	100–500 kHz	Signal attenuation can surpass 30 dB	Medium Voltage Powerline
Borges [34]	Capacitive Coupling	9 kHz to 500 kHz	Amplification is needed; simulation does not account for the integrated drain coil of the coupling capacitor, which impacts signal attenuation levels at the low frequencies of the CENELEC-A band.	Simulation only, no laboratory or field testing conducted
Masood [22]	Capacitive Coupling	12 kHz bandwidth (68 to 80 kHz)	Low Bandwidth (Varying attenuation)	Low and Medium Voltage (Used for channel measurements)
This Work	Capacitor with Drain Coil (Designed for higher BB PLC frequencies)	9 kHz to 500 kHz (Coupler); 19 kHz to 500 kHz (Coupler); 27 kHz to 440 kHz (Coupler + attenuator + filter + amplifier)	−46.5 dB (Coupler); −35 dB (Coupler); −50 dB to + 0 dB (Coupler + attenuator + filter + amp)	Receive Only. Impedance divider circuit trades off gain for bandwidth. Can cover the entire CENELEC and FCC frequency range

as a coupling device (filter) for the injection and reception of PLC signals on high-voltage overhead lines and cables. It incorporates a fourth-order high-pass filter that can be programmed for various values of coupling capacitance. Referring to the formulae given in [53], the upper-frequency limit can be calculated for a given lower-frequency limit. For a 19 kHz lower frequency limit and assuming the use of the same 5.1 nF CC, the upper-frequency limit is calculated as only 29.9 kHz for an insertion loss of 12 dB (only 11 kHz bandwidth). With a lower frequency limit set at 30 kHz, the upper frequency limit for the MCD80 extends only to 70 kHz, underscoring that it cannot match the wide frequency range nor the flexibility of the lower frequency limit of our design (9 kHZ). From a cost perspective, the proposed CoC design is over 80% cheaper than the retail price of MCD80, despite MCD80 not incorporating an active amplifier stage. The second off-the-shelf PLC tuning unit [54] states that it supports a limited frequency range of 40 to 500 kHz, which falls short of the targeted lower frequencies (9 kHz and above) of the CENELEC-A band.

In contrast to comparable works in the literature, the CoC proposed herein uses the low-cost, off-the-shelf BB-PLC Coupling Capacitor. It exploits the receive-only requirement of the line monitoring application to give a sliding trade-off between insertion loss and bandwidth. As demonstrated, working signal frequencies as low as 9 kHz become possible, giving the developed CoC prototype a bandwidth span of 19 kHz to 500 kHz. The CoC composes Stage 1 of an overall signal-conditioning circuit, which is followed by subsequent attenuation, filtering, and amplification stages to provide a flexible output control range of 50 dB.

9. Conclusions

The CENELEC-A band (9–95 kHz), reserved for power utilities, presents a challenge to cost-effective PLC-based applications aiming to access it without compromising bandwidth. This paper demonstrates that, for line monitoring and other receive-only applications, it is possible to trade off insertion loss for bandwidth without compromising carrier-to-noise ratio (CNR) with subsequent amplification. This is possible because the environmental noise in MV power lines is much higher than the noise present in the designed amplification stages. The design methodology for developing a CoC with a required low-frequency cut-off from an off-the-shelf encapsulated CC-drain coil unit is, therefore, the key contribution presented here. The analysis sections demonstrate how a CC developed for a higher frequency range (2 MHz to 30 MHz) can be made to operate at frequencies as low as 9 kHz. A LV series RC network, in parallel with the drain coil and a loading resistor, provides both a gain for the lower frequencies and control for the higher frequencies, enabling an overall flat response.

A prototype with a 19 kHz corner frequency has been tested in the lab and in the field, enabling communications over a heavily attenuated link on an MV SWER network. The use of lower loss low-frequency bandwidth allowed such transmission when previous attempts at higher frequencies (> 50 kHz) were not successful. The design methodology offers a procedure to achieve a large bandwidth (in drain-coil integrated capacitive coupling to the MV line) covering the entire CENELEC and

FCC bands. The methodology herein can potentially be adapted for customized designs dependent on the utilized CC. The insertion loss of the coupler (Stage 1) alone is approximately −46.5 dB for a 9 kHz to 500 kHz transmission range. When the signal conditioning board engages all of its stages (including the attenuator, filter, and amplifier), the insertion loss can be adjusted in the −50 dB to 0 dB range for a frequency range of 27 kHz to 440 kHz. The signal conditioning board was tested in the field over a week. The SNR was less than 0 dB for only 0.000148% of the time, and it was in the 20 dB to 40 dB range for 98.29% of the time. This validates the effectiveness of the proposed design in conditioning the signal, filtering out noise/interference, and providing proper impedance matching to maximize signal transfer. The key highlights of this research can be summarized as follows:

- Frequency Range: The signal conditioning circuit supports a frequency range from 9 kHz to 500 kHz, satisfying our primary objective of targeting transmission in the lower CENELEC-A band, given challenges in maintaining reliable transmission in overhead networks with underground sections.
- Design: An innovative design incorporating a series RC impedance in parallel with the drain coil of the utilized CC was used to create a resonant circuit, lowering the cut-off frequency to a lower desired value.
- Flexibility: When the attenuator, filter, and amplifier stages are engaged, the range can be adjusted from 27 kHz to 440 kHz, with an insertion loss that can be adjusted in the −50 dB to +0 dB range via attenuator and amplifier gain selections.
- Field validation: Extensive field tests validated an SNR exceeding 0 dB for 99.9999% of the time over a week period, with 98.29% of measurements in the 20 dB to 40 dB SNR range.
- Cost: The design represents a significantly more economical solution compared to off-the-shelf products available in the market while uniquely supporting reception in the lower CENELEC-A frequencies.

The proposed CoC solution demonstrates scalability for larger or more complex networks. Its modular architecture utilizes commercially available components and network integration through coupling capacitors (CCs), offering a cost-effective solution. Modular stages like attenuators and amplifiers can be independently added, removed, or upgraded, allowing for flexible adjustments to meet network requirements. Given that one CoC would be required at each receiving location, the cost to scale the system should grow only linearly with added capacity. Once designed for the CC of choice, new installations should ideally use the same CC for seamless integration and compatibility. A limitation of this work is the insufficient discussion on inductive coupling, which may be a cheaper alternative to CC-based coupling in medium voltage networks. The authors intend to address this shortcoming in future publications through an in-depth analysis of the use of inductive coupling in SWER networks as well as the design of dedicated signal conditioning circuits for such a coupling alternative.

CRediT authorship contribution statement

Kristi Beqirllari: Writing – original draft, Visualization, Software, Methodology, Investigation, Funding acquisition, Formal analysis, Data curation, Conceptualization. **Cagil Ozansoy:** Supervision, Funding acquisition, Conceptualization. **Douglas Gomes:** Writing – review & editing, Data curation. **Mike Faulkner:** Writing – review & editing, Formal analysis, Conceptualization.

Declaration of competing interest

The authors declare that they have no known competing financial interests or personal relationships that could have appeared to influence the work reported in this paper.

References

[1] D. Liang, Z. Wang, H. Liu, K. Zhang, Y. Wang, A novel online monitoring method of ground fault in tree form distribution networks based on power line carrier devices, Energy Rep. 9 (2023) 5287–5298, http://dx.doi.org/10.1016/j.egyr.2023.04.354.

[2] H. Loschi, D. Nascimento, R. Smolenski, W.E. Sayed, P. Lezynski, Shaping of converter interference for error rate reduction in PLC based smart metering systems, Measurement 203 (2022) 111946, http://dx.doi.org/10.1016/j.measurement.2022.111946.

[3] G. Lima, A. De Conti, Narrowband PLC channel attenuation due to a multi-grounded neutral, IEEE Trans. Power Deliv. 36 (2) (2021) 639–650.

[4] H. Ducloux, L. Figueroa, Background information about the wind action model of CENELEC EN 50341-1 (2012) and associated expected reliability of electrical overhead lines, J. Wind Eng. Ind. Aerodyn. 157 (2016) 104–117, http://dx.doi.org/10.1016/j.jweia.2016.08.006.

[5] Y.F. Coutinho, A. Camponogara, M. Filomeno, M. Campos, A.M. Tonello, M.V. Ribeiro, Two decades of research progress in resource allocation for PLC systems: From core concepts to frontiers, IEEE Commun. Surv. Tutor. (2024) http://dx.doi.org/10.1109/COMST.2024.3380901.

[6] G. López, J. Matanza, D. De La Vega, M. Castro, A. Arrinda, J.I. Moreno, A. Sendin, The role of power line communications in the smart grid revisited: Applications, challenges, and research initiatives, IEEE Access 7 (2019) 117346–117368.

[7] J. Yaacoub, J. Fernandez, H. Noura, A. Chehab, Security of power line communication systems: Issues, limitations and existing solutions, Comp. Sci. Rev. 39 (2021) 100331.

[8] B. Wang, Z. Cao, A review of impedance matching techniques in power line communications, Electronics 8 (9) (2019) 1022, http://dx.doi.org/10.3390/electronics8091022.

[9] L. Costa, C. Queiroz, B. Adebisi, V. Costa, M. Ribeiro, Coupling for power line communication: A survey, IEEE Commun. Surv. Tutor. (2024) http://dx.doi.org/10.1109/COMST.2024.3380901.

[10] M. Seijo, G. López, J. Matanza, J. Moreno, Planning and performance challenges in power line communications networks for smart grids, 2023.

[11] M. Wasowski, T. Sikorski, G. Wisniewski, P. Kostyla, J. Szymanda, M. Habrych, L. Gornicki, J. Sokol, M. Jurczyk, The impact of supply voltage waveform distortion on non-intentional emission in the frequency range 2–150 kHz: An experimental study with power-line communication and selected end-user equipment, Electronics 14 (2021) 777.

[12] I. Fernandez, L. Martínez, C. Rodríguez, Measurement system of the mean and sub-cycle LV grid access impedance from 20 kHz to 10 MHz, IEEE Trans. Power Deliv. (2023) 1–9, Article in Press.

[13] W. de Sousa Costa, R. da Silva Lima, Power line communication based SmartPlug prototype for power consumption monitoring in smart homes, IEEE Lat. Am. Trans. 19 (11) (2021) 1849–1857.

[14] P.A.J. van Rensburg, A.J. Snyders, H.C. Ferreira, Modeling of coupling diversity for extra-low-voltage power-line communication networked LED lighting in smart buildings, IEEE J. Emerg. Sel. Top. Power Electron. 6 (3) (2018) 1224–1234.

[15] J. Nguimbis, F. Labeau, P. Mabiala, Coupling unit topology for optimal signaling through the low-voltage powerline communication network, IEEE Trans. Power Deliv. 19 (3) (2004) 1065–1071, http://dx.doi.org/10.1109/TPWRD.2004.829910.

[16] P. v. Rensburg, H. Ferreira, A.J. Snyders, Coupler winding ratio selection for effective power transfer to a power-line communications receiver, in: IEEE International Symposium on Power Line Communications and Its Applications, Orlando, FL, USA, 2006, pp. 290–295.

[17] P. v. Rensburg, H. Ferreira, Design and evaluation of a dual impedance-adapting power-line communications coupler, IEEE Trans. Power Deliv. (2010) 667–673.

[18] S. Raponi, P. Falcone, Long-term noise characterization of narrowband power line communications measurements, analysis and modeling, IEEE Trans. Power Deliv. 37 (1) (2022) 365–373.

[19] S. Galli, A. Scaglione, Z. Wang, For the grid and through the grid: The role of power line communications in the smart grid, Proc. IEEE 99 (6) (2011) 998–1027.

[20] M. Yigit, V.C. Gungor, G. Tuna, M. Rangoussi, E. Fadel, Power line communication technologies for smart grid applications: A review of advances and challenges, Comput. Netw. 70 (2014) 366–383.

[21] L. Lampe, A.M. Tonello, T.G. Swart, Power Line Communications: Principles, Standards and Applications from Multimedia to Smart Grid, second ed., John Wiley & Sons Ltd, 2016.

[22] B. Masood, X. Liu, A. Yarali, Measurements and channel modeling of low and medium voltage NB-PLC networks for smart metering, IET Gener. Transm. Distrib. 14 (2020) http://dx.doi.org/10.1049/iet-gtd.2020.1233.

[23] T.F.A. Nogueira, F. Silva, R. Abreu, Inductive coupling-based narrowband PLC systems for overhead MV power distribution networks: New insights, Int. J. Electr. Power Energy Syst. 147 (2023).

[24] P.V. Rensburg, B. Watkins, S. Alahakoon, Design of a current-transformer based inductive coupler for power-line communications, IEEE Trans. Power Deliv. 38 (3) (2023) 1788–1798.

[25] K. Sohn, S. Yang, J. Jeong, Inductive coupling characteristics of nano-crystalline alloy for electric vehicle PLC, in: Proc. IEEE 10th International Conference on Ubiquitous Future Networks, 2018, pp. 543–545.
[26] K. Sohn, S. Yang, J. Jeong, K. Han, J. Moon, Experiments of in-vehicle inductive high-voltage power line communication, in: Proc. IEEE 11th International Conference on Ubiquitous Future Networks, 2019, pp. 601–603.
[27] H.-S. Kim, J.-H. Jo, C.-M. Lim, Signal transmission properties of the inductive coupler using the high permeability magnetic materials, J. Korean Inst. Electr. Electron. Mater. Eng. 19 (4) (2006) 339–343.
[28] A. Caprara, G. Ciotti, F. Bartoloni, On-line and off-line partial discharge scouting on MV networks, in: 2020 International Symposium on Electrical Insulating Materials, ISEIM, Tokyo, Japan, 2020.
[29] A. Cataliotti, V. Cosentino, D.D. Cara, G. Tine, Simulation and laboratory experimental tests of a line to shield medium-voltage power-line communication system, IEEE Trans. Power Deliv. 26 (4) (2011) 2829–2836, http://dx.doi.org/10.1109/TPWRD.2011.2166813.
[30] C.J. Kikkert, D. Perutka, Calculating radiation from power lines for power line communications, in: MATLAB for Engineers Applications in Control, Electrical Engineering, IT and Robotics, 2011.
[31] C. Kikkert, Effect of couplers and line branches on PLC communication channel response, in: IEEE International Conference on Smart Grid Communications, 2011.
[32] C. Kikkert, MV to LV transformer PLC bypass coupling networks for a low cost smart grid rollout, in: Innovative Smart Grid Technologies, Asia, 2011.
[33] L.G. da Silva Costa, B. Adebisi, V. Costa, M. Ribeiro, An augmented capacitive coupling circuit for boosting PLC systems in IoT domains, in: 2023 Symposium on Internet of Things (SIoT), São Paulo, Brazil, 2023, pp. 1–5, http://dx.doi.org/10.1109/SIoT60039.2023.10390135.
[34] M.V. Borges, G.H.B. Goncalves, L.G. da Silva Costa, A. Camponogara, M.J.C. do Couto Bonfim, M.V. Ribeiro, Active-based capacitive coupling circuit for narrowband PLC systems, in: 41st Brazilian Symposium on Telecommunications and Signal Processing, SBrT 2023, 2023.
[35] K. Razazian, M. Umari, A. Kamalizad, V. Loginov, M. Navid, G3-PLC specification for powerline communication: Overview, system simulation and field trial results, in: ISPLC2010, Rio de Janeiro, Brazil, 2010.
[36] E.F. da Costa, F.E. Nallin, Customized narrowband PLC system for medium-voltage distribution lines, Int. J. Sci. Eng. Investig. 8 (91) (2019).
[37] B. Martinez, N. Cante, M. Limas, F. Sierra, J. Becerra, Design of a T-coupling circuit for PLC on broadband, in: Proceedings of the IEEE Colombian Conference on Communications and Computing, 2014, pp. 1–6.
[38] S.S. Ali, A. Bhattacharya, D.R. Poddar, Design of bidirectional coupling circuit for broadband power-line communications, J. Electromagn. Anal. Appl. 4 (4) (2012).
[39] G. Artale, A. Cataliotti, V. Cosentino, D. Cara, R. Fiorelli, S. Guaiana, A new low cost coupling system for power line communication on medium voltage smart grids, IEEE Trans. Smart Grid 3321 (9) (2016) 9.
[40] G. Artale, A. Cataliotti, V. Cosentino, S. Guaiana, D. Cara, G. Tine, Development of a coupling system for medium voltage power line communication in the CELENEC a frequency band, in: IEEE International Workshop on Applied Measurements for Power Systems, 2020, pp. 1–6.
[41] G. Artale, A. Cataliotti, V. Cosentino, D. Di Cara, V. Ditta, S. Guaiana, N. Panzavecchia, G. Tine, Characterization and design of a PLC coupling system based on capacitive divider embedded in MV cable head, IEEE Trans. Power Deliv. PP (99) (2024) 1–11, http://dx.doi.org/10.1109/TPWRD.2024.3366419.
[42] A. Cataliotti, D.D. Cara, R. Fiorelli, G. Tine, Power-line communication in medium-voltage system: Simulation model and onfield experimental tests, IEEE Trans. Power Deliv. 27 (1) (2012) 62–69.
[43] H.-M. Oh, S. Choi, J.-J. Lee, S. Shon, H.S. Kim, D. Seok, Coupler with transformer for impedance matching on mv power distribution line for BPLC, in: 2008 IEEE International Symposium on Power Line Communications and Its Applications, 2008, pp. 409–412.
[44] D.-E. Lee, D.-S. In, J.-J. Lee, Y.-J. Park, K.-H. Kim, J.-T. Kim, S.-G. Shon, A field trial of medium voltage power line communication system for amr and DAS, in: Transmission & Distribution Conference & Exposition: Asia and Pacific, 2009.
[45] R. Benato, R. Caldon, Application of PLC for the control and the protection of future distribution networks, in: IEEE International Symposium, 2007.
[46] J.-J. Lee, S. Choi, S. Shon, H.S. Kim, D.S. In, J.-S. Park, Analysis of impedance characteristics of MV power distribution line for BPLC, in: 2008 IEEE International Symposium on Power Line Communications and Its Applications, 2007, pp. 24–29.
[47] J. Glover, M. Sarma, Power System Analysis and Design, Brooks/Cole Publishing Co., 2001, pp. 269–608.
[48] N. Watson, J. Arrillaga, Power Systems Electromagnetic Transients Simulation, Institution of Engineering and Technology, 2018.
[49] B. Nkom, A.P.R. Taylor, C. Baguley, Narrowband modeling of single-wire earth return distribution lines, IEEE Trans. Power Deliv. 33 (4) (2018) 1565–1575, http://dx.doi.org/10.1109/TPWRD.2017.2775189.
[50] IEEE, IEEE Std 1901.2: standard for low-frequency (less than 500 khz) narrowband power line communications for smart grid applications, 2013, IEEE Std 1901.2.
[51] IEEE, IEEE Std C93.4-2012: standard for power-line carrier line-tuning equipment (30 khz to 500 khz) associated with power transmission lines, 2013, pp. 1–67, http://dx.doi.org/10.1109/IEEESTD.2013.6471993.
[52] Victoria university: SWER broken conductor detection stage 2 - final report, 2013, (Accessed 9 November 2023), https://www.energy.vic.gov.au/_data/assets/pdf_file/0014/602321/9cc72d9135acce10949d669ac8eeace25cbe1eee.pdf.
[53] ABB, MCD80 power line carrier coupling device, 2011, URL https://library.e.abb.com/public/770253b1432c43f1966eacafaaf0ba49/MCD80_2011_Lowres.pdf?x-sign=bc5f03GGPNyLoC5bijhXA2CuJlcyk8YVhJH/8zGn1pCc6ig5bNQSzeWlLytmHmhL, (Accessed 03 July 2024).
[54] R. Electronics, RFL 9512 product information, 2024, URL https://www.rflelect.com/images/products/pdfs/RFL_9512_RFLprint_updated.pdf, (Accessed 04 July 2024).